

# Hierarchical Assembly and Compliance of Aligned Nanoscale Polymer Cylinders in Confinement

Deepak Sundrani,<sup>†</sup> S. B. Darling,<sup>‡</sup> and S. J. Sibener<sup>\*,†</sup>

The James Franck Institute and the Department of Chemistry, The University of Chicago, 5640 South Ellis Avenue, Chicago, Illinois 60637, and Materials Science Division, Argonne National Laboratory, 9700 South Cass Avenue, Argonne, Illinois 60439

Received November 11, 2003. In Final Form: January 29, 2004

We report a combined top-down/bottom-up hierarchical approach to fabricate massively parallel arrays of aligned nanoscale domains by means of the self-assembly of asymmetric polystyrene-*block*-poly(ethylene-*alt*-propylene) diblock copolymers. Silicon nitride grating substrates of various depths and periodicities are used to template the alignment of the high-aspect-ratio cylindrical polymer domains. Alignment is nucleated by polystyrene preferentially wetting the trough sidewalls and is thermally extended throughout the polymer film by defect annihilation. Topics discussed include a detailed analysis of the capacity of this system to accommodate lithographic defects and observations of alignment beyond the confined channel volumes. This graphoepitaxial methodology can be exploited in hybrid hard/soft condensed matter systems for a variety of applications.

## Introduction

The success of nanotechnology hinges on the ability to rationally arrange functional materials on the nanoscale. Traditionally, this has been achieved by top-down lithographic processes, but fundamental limitations associated with these techniques are rapidly becoming apparent. Not only is lithography hitting the lower limit of its length scale capability at  $\sim 20$  nm, but also the process itself is often inefficiently serial in nature. Bottom-up self-assembly has the capacity to transcend both of these limitations because it is inherently parallel and uses molecules as the building blocks to enter the nanoscale. Most hard materials, however, will not self-organize at these length scales. For this reason, hybrid systems where soft matter self-organizes into a nanoscale template that directs the assembly of hard matter are promising. Nevertheless, pure bottom-up methods have their own drawback: one cannot attain long-range order. The solution to this dilemma is to adopt a hierarchical, combination top-down/bottom-up methodology.

Diblock copolymers are compelling candidates for the bottom-up component because of the accessibility of diverse structures with tunable length scales. Depending on the relative chain lengths of the two polymer blocks, these systems phase separate into nanoscale spheres, cylinders, gyroids, or lamellae. Simply adjusting the molecular weight of the polymer scales the resultant structural phases proportionally. Several groups have studied the lithographically assisted self-assembly of the spherical phase. Kramer and co-workers were the first to demonstrate a graphoepitaxial strategy for creating single-crystal films of block copolymers over large areas of a substrate.<sup>1</sup> Ross and co-workers extended this work to more confined volumes and identified the effect of lithographic defects and the relation of channel width and polymer sphere accommodation.<sup>2,3</sup>

\* To whom correspondence should be addressed. E-mail: s-sibener@uchicago.edu.

<sup>†</sup> The University of Chicago.

<sup>‡</sup> Argonne National Laboratory.

(1) Segalman, R. A.; Yokoyama, H.; Kramer, E. J. Graphoepitaxy of Spherical Domain Block Copolymer Films. *Adv. Mater.* **2001**, *13*, 1152–1155.

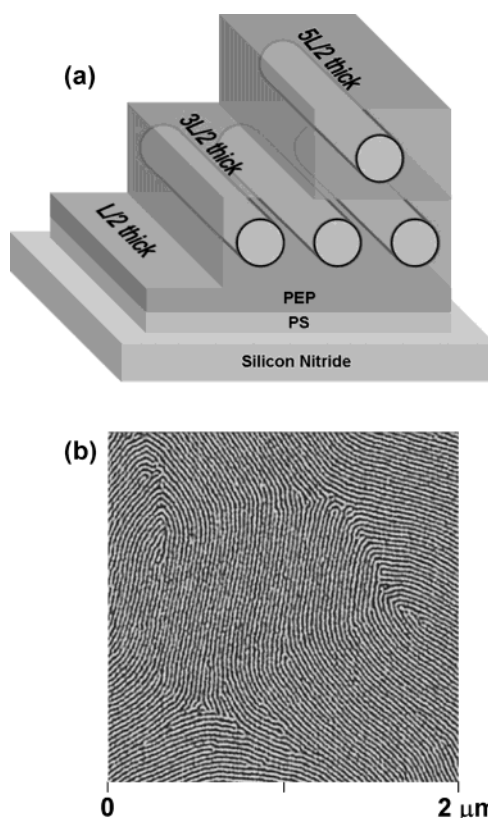


**Figure 1.** (a) Schematic of a PS-*b*-PEP thin film organizing on a silicon nitride substrate. PS, in light shading, prefers to wet the substrate/polymer interface whereas PEP, in dark shading, prefers to wet the polymer/air interface. For films of  $L/2$  thickness, the surface is featureless as a result of the absence of underlying PS cylinders. In films that are thicker than  $L/2$ , the underlying PS cylinders in the PEP matrix organize as a disordered fingerprint structure. (b) Tapping mode phase AFM image,  $2 \mu\text{m} \times 2 \mu\text{m}$ , showing fingerprint pattern of microphase-separated domains typically observed on a flat substrate. This sample, prepared by spin-coating the 1.55% polymer solution at 5 krpm and then annealing at 403 K for 24 h, has no preferential orientation of cylinders. The bright domain is PS, and the dark domain is PEP.

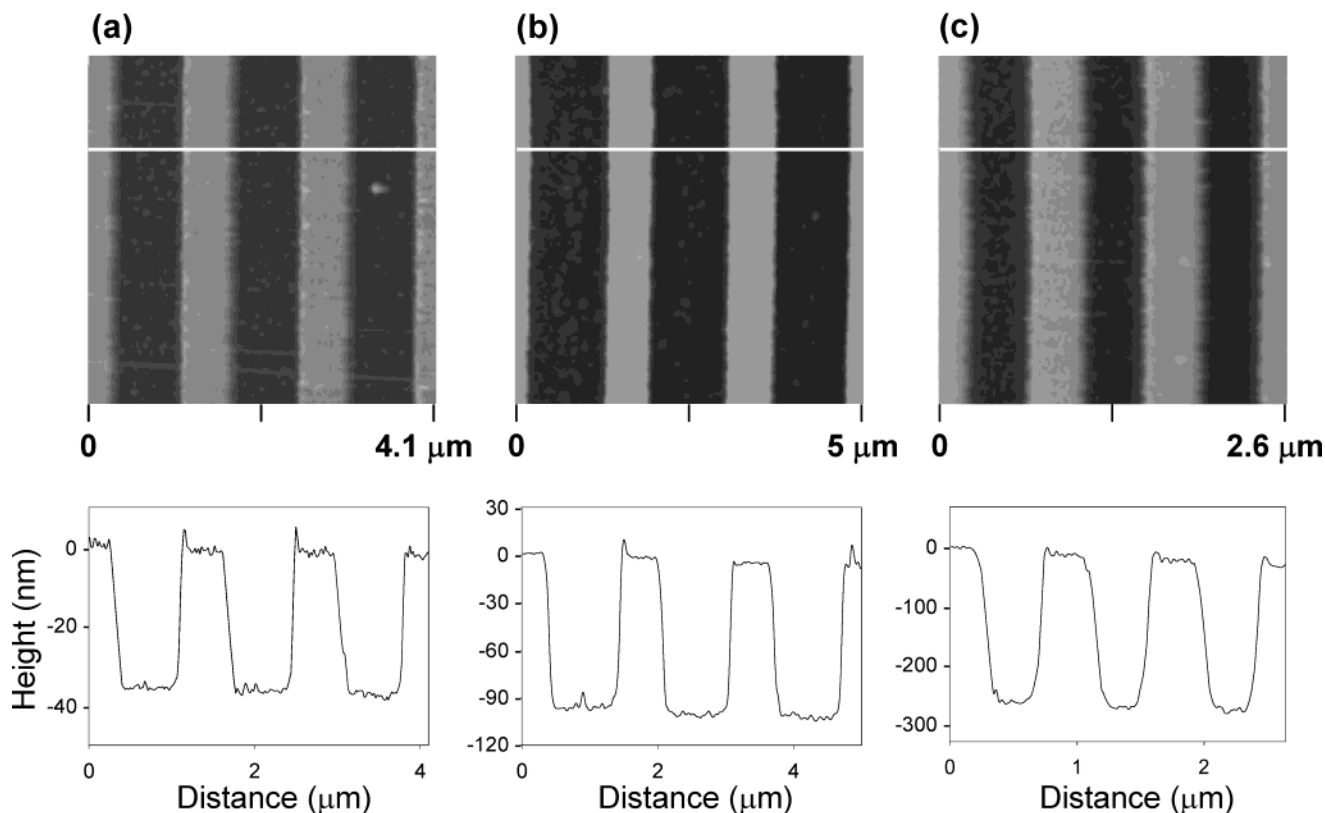


**Figure 2.** Tapping mode topographic AFM images of bare silicon nitride gratings of corrugation (a)  $\sim 35$  nm ( $4.1 \mu\text{m} \times 4.1 \mu\text{m}$ ), (b)  $\sim 95$  nm ( $5 \mu\text{m} \times 5 \mu\text{m}$ ), and (c)  $\sim 280$  nm ( $2.6 \mu\text{m} \times 2.6 \mu\text{m}$ ). Height profiles of the inserted lines show the square-wave structure of the gratings, where zero corresponds to the clean, unetched substrate plane.

While the spherical phase has potential for applications such as high-density magnetic recording,<sup>4,5</sup> the exceedingly large aspect ratio, that is, the potentially macroscopic extent of the cylinder length compared to the nanoscale repeat distance for cylindrical phase structures, opens the door to applications in electronics, optics, and sensor technology when using cylinder-forming materials. Harnessing this potential has been hindered by the fact that thin films of the cylindrical phase form disordered fingerprint patterns. Attempts to induce order in such films using electric fields,<sup>6</sup> solvent prewetting,<sup>7</sup> and directional crystallization<sup>8</sup> have seen moderate success, but all suffer from one or more of the following shortcomings: no long-range order, no control over the location or orientation of ordered domains, and nonparallel cylinder formation. In this article, we report a novel and general

method that overcomes all of these obstacles. Our approach begins by preparing a silicon nitride grating substrate using electron beam lithography and reactive ion etching. This grating is then used to guide the assembly of polymer cylinders along the length of the etched channels. Compliance of the cylinder size and spacing to variations in the trough width is discussed, and because defect tolerance is critical in creating a near-perfect and robust nanotemplate, the role of defects is also reviewed.

### Experimental Procedure

Asymmetric polystyrene-*block*-polyisoprene (PS-*b*-PI), obtained from Polymer Source, Inc. (Dorval, Quebec, Canada), was 27 wt % PS with a molecular weight of 22 000 g/mol and polydispersity of 1.08. Homogeneous Ni–Al catalyst<sup>9,10</sup> was used to selectively hydrogenate the isoprene block to prepare polystyrene-*block*-poly(ethylene-*alt*-propylene) (PS-*b*-PEP). This hydrogenated polymer was used for these experiments because its structure has been characterized and its relatively low glass temperature is conducive to time-resolved microscopy measurements.<sup>11</sup>

Silicon nitride gratings, containing square-wave grating patterns, were prepared in a silicon nitride layer by electron beam lithography using a Hitachi S-2700 scanning electron microscope and reactive ion etching. The size of the grating pattern on these topographically patterned substrates is  $100 \mu\text{m} \times 100 \mu\text{m}$ . Each grating contained troughs of different widths

(2) Cheng, J. Y.; Ross, C. A.; Thomas, E.; Smith, H. I.; Vancso, G. J. Fabrication of nanostructures with long-range order using block copolymer lithography. *Appl. Phys. Lett.* **2002**, *81*, 3657–3659.

(3) Cheng, J. Y.; Ross, C. A.; Thomas, E. L.; Smith, H. I.; Vancso, G. J. Templated Self-Assembly of Block Copolymers: Effect of Substrate Topography. *Adv. Mater.* **2003**, *15*, 1599–1602.

(4) Asakawa, K.; Hiraoka, T.; Hieda, H.; Sakurai, M.; Kamata, Y.; Naito, K. Nano-patterning for patterned media using block-copolymer. *J. Photopolym. Sci. Technol.* **2002**, *15*, 465–470.

(5) Cheng, J. Y.; Ross, C. A.; Thomas, E. L.; Smith, H. I.; Lammertink, R. G. H.; Vancso, G. J. Magnetic properties of large-area particle arrays fabricated using block copolymer lithography. *IEEE Trans. Magn.* **2002**, *38*, 2541–2543.

(6) Morkved, T. L.; Lu, M.; Urbas, A. M.; Ehrichs, E. E.; Jaeger, H. M.; Mansky, P.; Russell, T. P. Local Control of Microdomain Orientation in Diblock Copolymer Thin Films with Electric Fields. *Science* **1996**, *273*, 931–933.

(7) Hahn, J.; Sibener, S. J. Cylinder Alignment in Annular Structures of Microphase-Separated Polystyrene-*b*-Poly(methyl methacrylate). *Langmuir* **2000**, *16*, 4766–4769.

(8) Park, C.; Rosa, C. D.; Thomas, E. L. Large Area Orientation of Block Copolymer Microdomains in Thin Films via Directional Crystallization of a Solvent. *Macromolecules* **2001**, *34*, 2602–2606.

(9) Adams, J. L.; Quiram, D. J.; Graessley, W. W.; Register, R. A.; Marchand, G. R. Interaction Strengths in Styrene-Diene Block Copolymers and Their Hydrogenated Derivatives. *Macromolecules* **1998**, *31*, 201–204.

(10) Sundrani, D.; Zheng, Q.; Lee, D.-C.; Yu, L.; Sibener, S. J. *Macromolecules*, submitted for publication.

(11) Harrison, C.; Cheng, Z.; Sethuraman, S.; Huse, D. A.; Chaikin, P. M.; Vega, D. A.; Sebastian, J. M.; Register, R. A.; Adamson, D. H. Dynamics of pattern coarsening in a two-dimensional smectic system. *Phys. Rev. E* **2002**, *66*, 011706-1–011706-27.

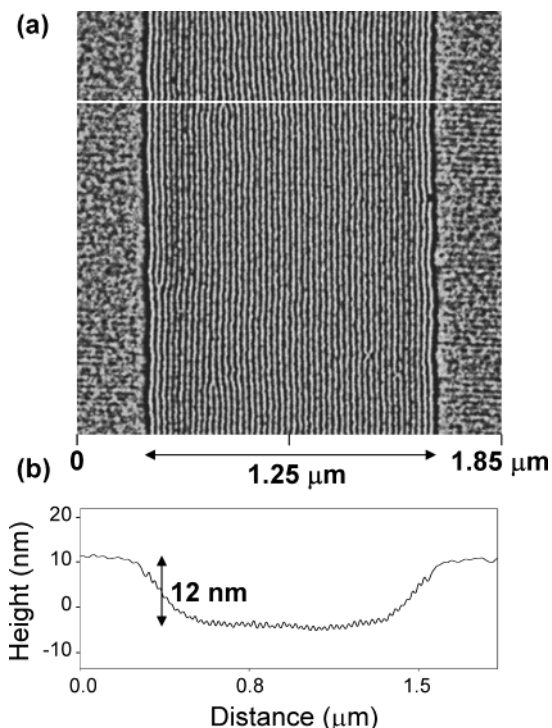


**Figure 3.** (a) Tapping mode phase AFM image,  $1.85 \mu\text{m} \times 1.85 \mu\text{m}$ , of a thin film sample prepared by spin-coating the 1.55% polymer solution at 5 krpm on a 35-nm-deep grating. The preferential interaction of PS (not imaged because it is deeply submerged) with the trough sidewalls aligns cylinders along the edges. The trough is  $1.25\text{-}\mu\text{m}$ -wide and it has a  $3L/2$ -thick (35 nm) film. Annealing at 403 K for 24 h aligns the cylinders parallel to the grating lines across the entire trough width and along the full  $100\text{-}\mu\text{m}$  length. Crests are covered with an  $L/2$ -thick film and, therefore, appear featureless. (b) The height profile of the inserted line in part a, shows a corrugation of 12 nm from the crests to the troughs, where zero corresponds to the clean, unetched substrate plane.

ranging from 200 nm to  $1.5 \mu\text{m}$  in increments of 100 nm; the trough length was always  $100 \mu\text{m}$ . Crest widths were a constant  $\sim 750$  nm. Gratings of three different depths,  $\sim 35$ ,  $\sim 95$ , and  $\sim 280$  nm, were used for these experiments.

The gratings were cleaned with trichloroethylene, hot toluene, acetone, and methanol (in this order) using an ultrasonic cleaner. Substrates were kept submerged in methanol until thin films of diblock copolymer were to be deposited. Before being coated with a polymer film, the gratings were dried with ultrahigh purity nitrogen. We have found that including a further preparation step produces the cleanest possible substrate and, subsequently, the most uniform polymer films. On the washed gratings, a thin film of polystyrene-*block*-poly(methyl methacrylate) was deposited, annealed at 523 K for 6 h under an argon atmosphere, and stripped off using the cleaning procedure just mentioned. We believe that this step removes trace contaminants introduced during manufacture of the grating. Polymer films were prepared by placing a drop size in the range  $4\text{--}5 \mu\text{L}$  of 1.55% (w/w) PS-*b*-PEP/toluene solution on a grating and then spinning at selected speeds for 1 min. Subsequent thermal annealing of the samples was carried out at selected temperatures (388–408 K) under an argon atmosphere. Annealing was achieved by a transient ramp rate of 5 K/min from room temperature to the final temperature.

Atomic force microscopy (AFM) measurements were conducted to examine the resulting microphase separation behavior of diblock copolymer thin films. Tapping mode AFM was performed with silicon Nanoscope SPM tips (resonance frequency  $\sim 320$  kHz) using a Nanoscope IIIa/IV, Digital Instruments Multimode SPM. The presence of a featureless  $L/2 = \sim 12\text{-nm}$ -thick film ( $L$  is the natural thickness of one layer of cylinders) on the crests provides a reference to find the thickness of the film on the crests and in the troughs.

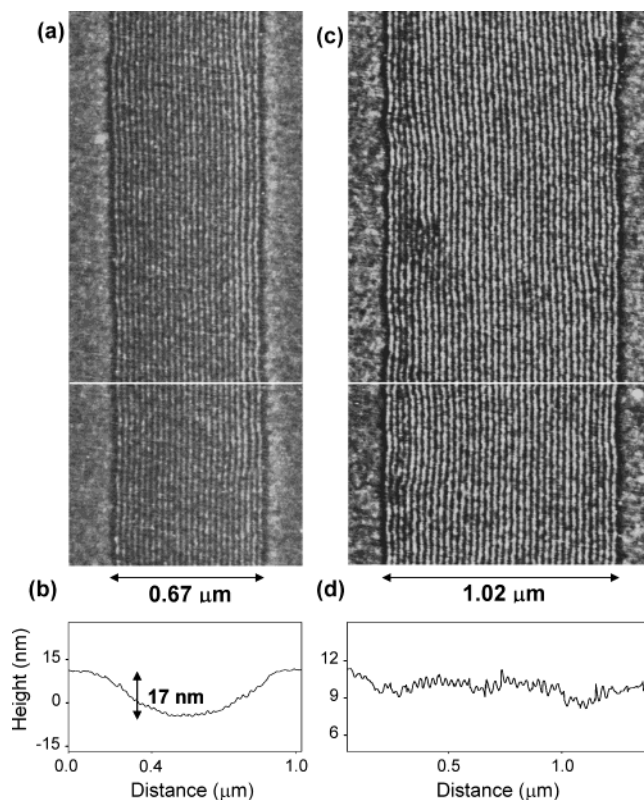


**Figure 4.** Thin film sample prepared by spin-coating the 1.55% polymer solution at 5 krpm on a 95-nm-deep grating. Annealing at 403 K for 30 h results in parallel alignment of cylinders in all the troughs. Tapping mode phase AFM images of two such troughs of widths  $0.67 \mu\text{m}$  and  $1.02 \mu\text{m}$  are shown in parts a and c, respectively. (b) The height profile of the inserted line in part a shows a corrugation of 17 nm from the crest to the trough. The trough in part a has a film thickness slightly greater than  $7L/2$ . (d) The height profile of the inserted line in part c shows a flat film in the trough; the corrugation from the crest to the trough is 2–3 nm, so the trough in part c has a  $9L/2$ -thick film. Zero in both profiles corresponds to the clean, unetched substrate plane.

## Results and Discussion

Three square-wave silicon nitride gratings of depths  $\sim 35$ ,  $\sim 95$ , and  $\sim 280$  nm were used as substrates to study the structure of spin-coated PS-*b*-PEP diblock copolymer thin films. The behavior of thin films on these corrugated substrates is compared with those grown on flat silicon nitride substrates. Asymmetric wetting of PS-*b*-PEP occurs on a silicon nitride substrate;<sup>11</sup> that is, PS prefers to wet the silicon nitride/polymer interface whereas PEP exhibits an affinity for the polymer/air interface (Figure 1a). Therefore, the film thickness is quantized to odd multiples of  $L/2$ , that is,  $(2n + 1)L/2$ , where  $n$  is an integer and  $L$  is 23 nm for PS-*b*-PEP of molecular weight 22 000 g/mol. The spacing between nearest-neighbor cylinders of PS hexagonally packed in the PEP matrix is 26.6 nm. A cylinder-free monolayer of diblock copolymer covers the substrate for a film of  $L/2$  thickness; therefore, the surface of an  $L/2$ -thick film appears featureless when it is imaged using tapping mode AFM. For films thicker than  $L/2$  ( $3L/2$ ,  $5L/2$ , etc.), the underlying PS cylinders parallel to the film plane appear as a disordered fingerprint structure (Figure 1b) when imaged with AFM under hard tapping conditions. The difference in the elastic moduli of PS and PEP results in the difference in contrast in the phase images; the bright domain is PS and the dark domain is PEP. This sample is prepared by spin-coating a 1.55%

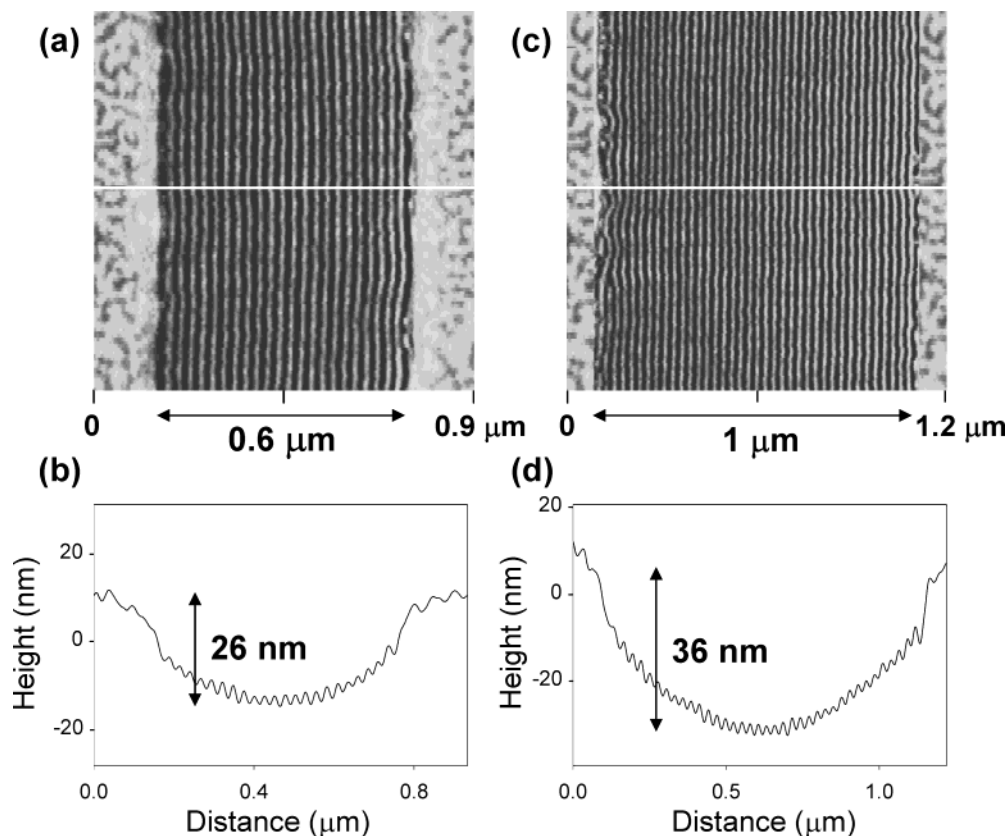


**Figure 5.** Thin film sample prepared by spin-coating the 1.55% polymer solution at 2.5 krpm on a 280-nm-deep grating and then annealing at 403 K for 45 h, resulting in parallel alignment of the cylinders in all the troughs. Tapping mode phase AFM images of two such troughs of widths 0.6 and 1  $\mu\text{m}$  are shown in parts a and c, respectively. (b) The height profile of the inserted line in part a shows a corrugation of 26 nm from the crest to the trough. (d) The height profile of the inserted line in part c shows a corrugation of 36 nm from the crest to the trough. The troughs in parts a and c have a  $\sim 23L/2$ -thick film. Zero in both profiles corresponds to the clean, unetched substrate plane.

polymer solution at 5 krpm on a flat silicon nitride substrate and then annealing at 403 K for 24 h. The average thickness of the spin-coated film is not equal to any quantized film thickness; hence, after annealing, islands and holes corresponding to  $5L/2$ -thick and  $3L/2$ -thick films, respectively, are formed on the surface. No preferential orientation of cylinders is observed in either the islands or the holes, and the domains contain numerous defects despite extensive annealing. This absence of long-range order is characteristic of films prepared on flat substrates.

**Polymer Films on the 35-nm-Deep Grating.** When a thin film is spin-coated on a grating, the corrugation of the substrate leads to deposition of nonuniform films. Higher coverage of polymer is observed in the troughs compared to the crests because the polymer can flow from the crests into the troughs during spin coating and subsequent annealing. Figure 2 shows topographic AFM images and height profiles of the gratings used in these experiments. From the height profiles it can be observed that the gratings have sharp edges.

The presence of the trough side walls and the nanoscale confinement of domains cause the cylinders to exhibit long-range order on these corrugated substrates. A thin film sample prepared by spin-coating the 1.55% polymer solution at 5 krpm on a 35-nm-deep grating, after annealing, has an  $L/2$ -thick film on the crests, whereas the troughs are completely filled with the polymer. The polymer film thickness in the troughs,  $\sim 35$  nm, corresponds to a film with only one layer of underlying PS cylinders. PS interacting preferentially with the trough sidewalls drives the alignment of cylindrical domains

parallel to the edges of the troughs.<sup>12</sup> The first imaged polymer domain along the trough edges appears wider because of the presence of a brush layer along the sidewalls. When the sample is annealed for 2 h, the alignment of one or two cylinders near the edges is observed. Further annealing leads to coarsening of these aligned domains, and after 24 h of annealing at 403 K, perfect parallel alignment of cylinders is present across the entire trough width. The cylinders are aligned along the complete 100- $\mu\text{m}$  length of all the troughs regardless of the width. Figure 3a shows the phase image of a 1.25- $\mu\text{m}$ -wide trough with perfectly aligned cylindrical domains. The troughs are almost completely filled with the polymer and they have a flat profile; the height difference of  $\sim 12$  nm from the crests to the troughs (Figure 3b) is attributable to the  $L/2$ -thick film present on the crests.

**Polymer Films on Deeper Gratings.** Alignment also occurs for gratings with higher corrugations of  $\sim 95$  and  $\sim 280$  nm. These troughs can comfortably accommodate polymer films of thickness  $7L/2$  and  $23L/2$ , that is, films with 3 and 11 layers of underlying PS cylinders, respectively. When a thin film is prepared on a 95-nm-deep grating by spin-coating the 1.55% polymer solution at 5 krpm and then annealing at 403 K for 30 h, the cylinders align parallel to the grating lines along the full 100- $\mu\text{m}$  length regardless of the channel width. Parts a and c of Figure 4 show this aligned structure for two 95-nm-deep

(12) Yokoyama, H.; Mates, T. E.; Kramer, E. J. Structure of Asymmetric Diblock Copolymers in Thin Films. *Macromolecules* **2000**, *33*, 1888–1898.

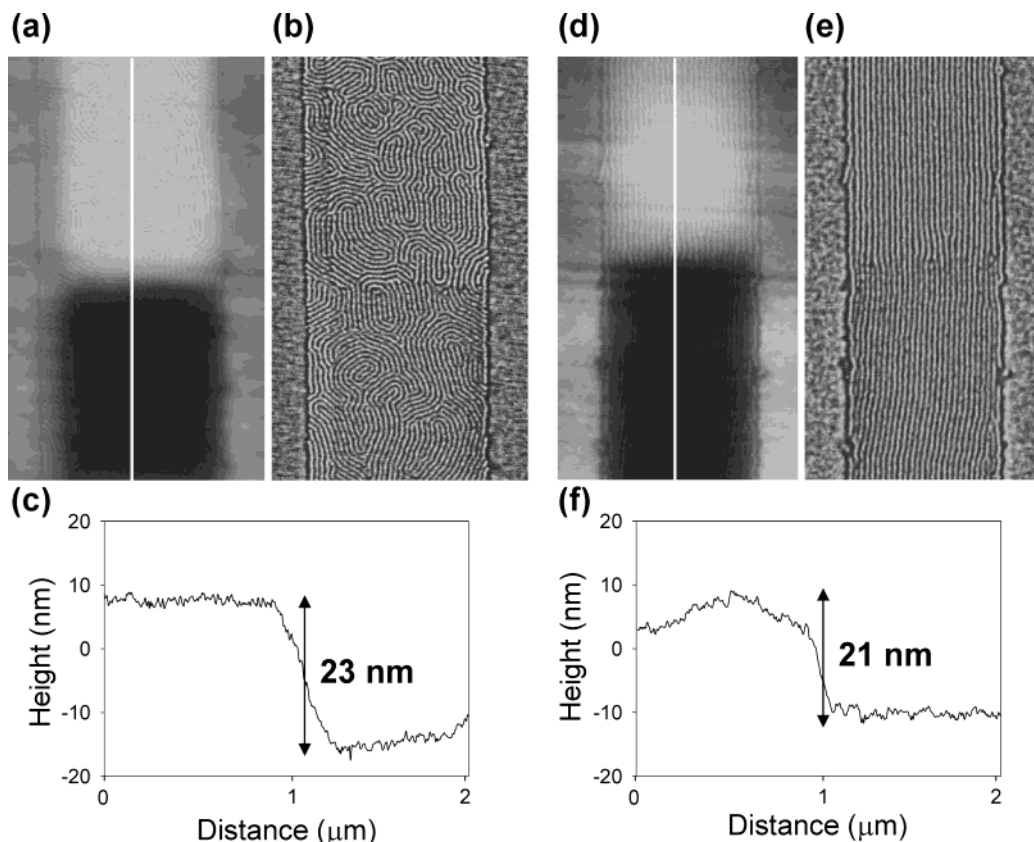


**Figure 6.** Thin film sample prepared by spin-coating the 1.55% polymer solution at 5 krpm on a 35-nm-deep grating. Tapping mode (a) topographic and (b) phase AFM images of the same region of the trough (960-nm wide) when the sample is annealed at 388 K for 2 h. The bright and dark regions in the trough in part a correspond to  $5L/2$ - and  $3L/2$ -thick films, respectively; therefore, (c) the height profile of the inserted line in part a shows a corrugation of 23 nm. Following brief annealing, cylinders in  $5L/2$ - and  $3L/2$ -thick regions have a disordered fingerprint structure. Tapping mode (d) topographic and (e) phase AFM images of another trough (800-nm wide) when the sample is further annealed at 403 K for 20 h. Now, the cylinders in the  $5L/2$ - and  $3L/2$ -thick regions in the trough in part d have perfect parallel alignment. The corrugation of 21 nm in the (f) height profile of the inserted line in part d supports the presence of  $5L/2$ - and  $3L/2$ -thick regions in the trough.

trenches of widths 0.67 and 1.02  $\mu\text{m}$ , respectively. The height profile for the narrower channel (Figure 4b) shows a corrugation of 17 nm from the  $L/2$ -thick film on the crest to the center of the trough. Despite the fact that the film is not of an ideal thickness and is not completely flat, perfect parallel alignment of cylinders is observed. In contrast to the 0.67- $\mu\text{m}$ -wide trough, the 1.02- $\mu\text{m}$ -wide trough is overfilled with polymer. Corrugation from the crest to the trough is 2–3 nm (Figure 4d); therefore, the polymer film in the trough is  $9L/2$ -thick (103 nm). Similar results are obtained with the 280-nm-deep grating (Figure 5). The observation of parallel alignment of cylinders for all gratings suggests that the depth of the troughs, if greater than 35 nm, is not critical. In fact, alignment was not observed for a grating of depth 25 nm ( $<3L/2$ ).

**Alignment Mechanism.** Time-lapse studies have been performed to observe the thermal alignment of cylinders.<sup>13</sup> These studies show that, at shorter annealing times, one or two cylinders align along the edges of the troughs, but the cylinders in the center of the channels are largely aligned across the troughs. This perpendicular alignment is due to cylinders aligning along the direction of polymer flow as it migrates from the crests into the troughs. Alignment of cylinders across the troughs due to capillary polymer flow from the center of the troughs to their edges has been reported,<sup>14</sup> but in this case, the

polymer flows in the reverse direction as the overall film flattens during annealing. Further annealing leads to coarsening of alignment across the full trough width at random locations along the troughs, and finally, these smaller perfected regions merge, resulting in perfectly aligned cylindrical domains along the entire channel length. The same mechanism for alignment is observed for all the trough widths studied. We have also observed that polymer can flow from the smooth part of the sample into the channels through the trough ends during annealing. This process helps to load the troughs that are unfilled after the initial film preparation. One might conclude that this parallel flow of polymer into the troughs could account for the parallel alignment of cylinders. This cannot be the case because (1) there is insufficient time during annealing for alignment to grow in only from the channel termini, (2) alignment has been observed to nucleate at many locations within the troughs, and (3) alignment is observed in channels where the ends were physically separated from the bulk of the channel length by material blockage.

Tapping mode AFM can only image the top layer of aligned cylinders, but the structure of cylinders underneath this layer may also be useful for understanding the overall mechanism of alignment. When a thin film is prepared by spin-coating (1.55% polymer solution at 5 krpm) on a 35-nm-deep grating, the sample has regions

(13) Sundrani, D.; Darling, S. B.; Sibener, S. J. Guiding polymers to perfection: Macroscopic alignment of nanoscale domains. *Nano Lett.* **2004**, *4*, 273–276.

(14) Sundrani, D.; Sibener, S. J. Spontaneous spatial alignment of polymer cylindrical nanodomains on silicon nitride gratings. *Macromolecules* **2002**, *35*, 8531–8539.

that have  $3L/2$ - (35 nm) and  $5L/2$ -thick films in the troughs. Parts a and b of Figure 6 show the topographic and phase images, respectively, of one such trough on this sample annealed at 388 K for 2 h. The bright region in the trough in Figure 6a corresponds to a  $5L/2$ -thick film, while the dark region corresponds to a  $3L/2$ -thick film. Both regions have a disordered fingerprint structure. Further annealing (403 K for 24 h) results in parallel cylinder alignment in both regions (Figure 6d,e). Although the top layer of cylinders in the  $5L/2$ -thick film is not confined in the trough, the occurrence of alignment in this layer suggests that underlying cylinders can align those in upper layers. The same phenomenon has been observed in films with many more cylinder layers. Figure 7a shows the phase image of parallel alignment of cylinders in a channel that has  $7L/2$ - (80 nm) and  $9L/2$ -thick (103 nm) regions. It is interesting to observe that cylinders in the top layer do not form dislocation dead ends at the island–hole boundary; on the other hand, they continue from the islands to the holes without introducing defects. This behavior illustrates the robustness of the confinement effect. Cylinders of PS are hexagonally packed in the PEP matrix in bulk copolymers. In this instance, the usual offset vertical packing of the cylinders is modified to a rectangular lattice either at these island–hole boundaries or throughout the channel volume. Further studies are in progress to decipher the packing of submerged cylinders in confinement.

**Polymer Compliance in Confined Volumes.** Cylindrical domains closely follow the variation in the trough width along its length by complying with the variations of the trough sidewall. Related behavior has been observed in spherical domain systems.<sup>3</sup> A plot of the number of PEP domains versus trough width is shown in Figure 8a. From this plot, it is clear that the same number of polymer domains is observed over a range of trough widths. The polymer conforms to its confined environment by varying the periodicity of the cylindrical domains. This range of trough widths available to a given number of domains increases with the number of domains; that is, each additional polymer domain introduces more flexibility into the system. Elasticity of the confined polymers is further demonstrated by the fact that there are also regions where a given trough width can accommodate more than one number of polymer domains. The polymer avoids creation of high-energy dislocation defects by expanding or contracting within the accessible range as necessary. At some point, this regulation becomes more costly than the energy required to create a dislocation and a single defect is formed. For example, the trough width of 300 nm can accommodate either 10 or 11 PEP domains; the actual number of domains depends on the history of the system. A 300-nm-wide channel favors 11 PEP domains (equilibrium size  $\sim 304$  nm), but if the majority of the channel is narrower, that is, closer to the width of 10 domains in equilibrium, it will accommodate the width variation without creating defects. The overlap between different numbers of polymer domains, too, increases with the number of domains present in the troughs. Figure 8b depicts a concrete illustration of how this flexibility minimizes the defect density in aligned structures. This image shows a 95-nm-deep trough of width 285 nm with a  $9L/2$  polymer film that has perfectly aligned cylindrical domains along its full 100- $\mu\text{m}$  length. The lithographically induced variation in the width of this trough along its length is within the accessible range for 11 PEP domains. Therefore, the cylindrical domains in this trough have a defect-free structure.

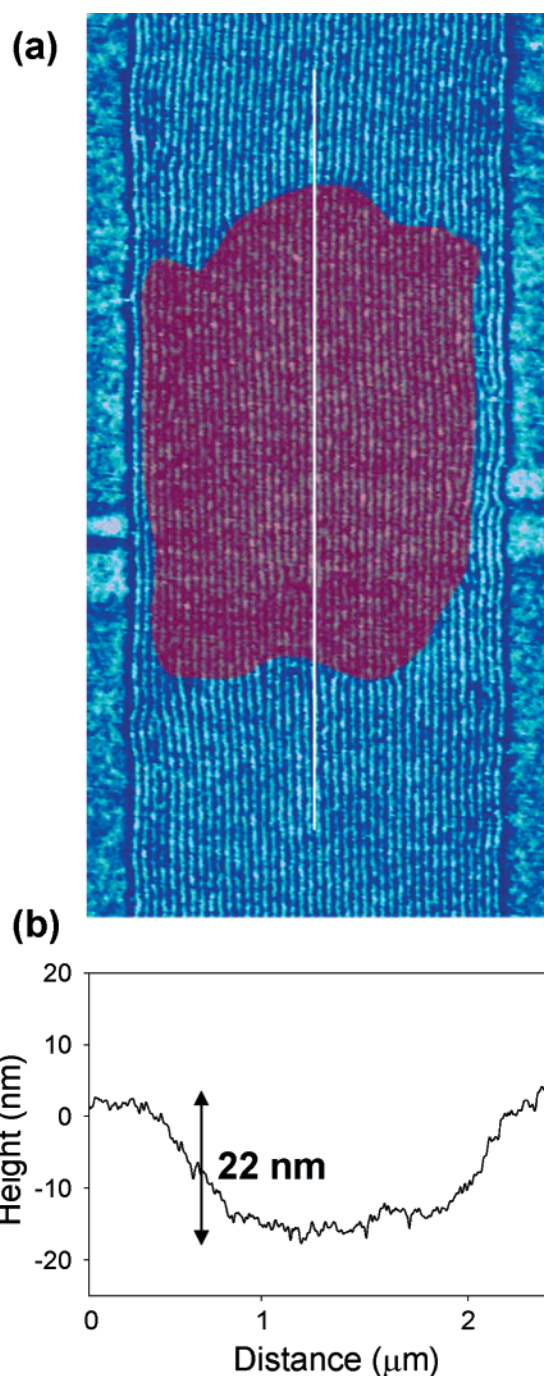


**Figure 7.** Thin film sample prepared by spin-coating the 1.55% polymer solution at 5 krpm on a 95-nm-deep grating and then annealing at 403 K for 30 h. (a) Tapping mode phase AFM image of a 1- $\mu\text{m}$  wide trough, which has islands ( $9L/2$  thick) and holes ( $7L/2$  thick, false red color). Again, the alignment is present in the  $9L/2$ - and  $7L/2$ -thick regions, and the cylinders cross the boundary with minimal introduction of defects. (b) The height profile of the inserted line in part a shows the corrugation of 22 nm from the islands to the holes.

If, though, the variation in the trough width is significant then a change in the number of polymer domains in the channel is observed. A specific illustration of this phenomenon follows. The trough shown in Figure 9 has 10 PEP polymer domains along the majority of its length; however, when the trough width exits the range available for 10 domains (Figure 8a), the number of polymer domains changes accordingly. Note that this sample was extensively annealed (403 K for 30 h), so the structure is close to thermodynamic equilibrium. Near spot A in Figure 9,

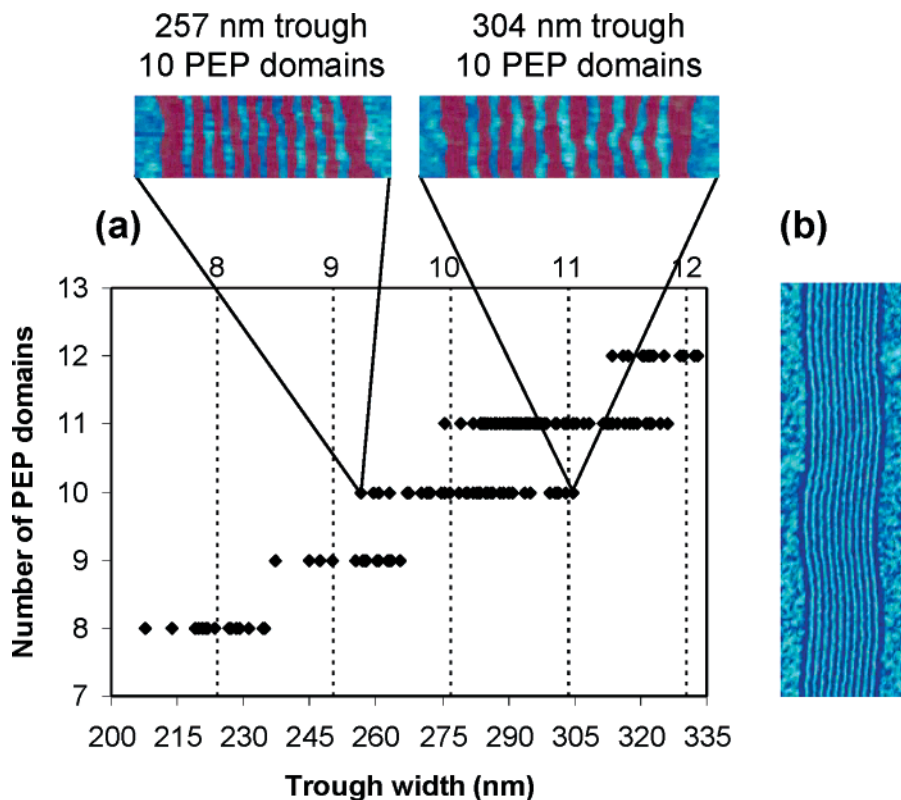


**Figure 8.** (a) Plot of the number of PEP polymer domains versus the trough width. For a range of trough widths, a constant number of polymer domains is observed. There is an overlap in the regions where the same trough width can accommodate more than one number of polymer domains. Integer multiples of the equilibrium, unconfined domain spacing of 26.6 nm plus the average thickness of the brush layer (25.6 nm), are denoted by dashed lines. Illustrative images (false red color) are shown for the minimum and maximum trough widths that can accommodate 10 PEP domains. The range of widths shown in this figure represents the full data range available; the trend of widening accommodation with increased number of PEP domains is expected to continue for 12 domains and beyond. (b) Tapping mode phase AFM image of a 95-nm-deep and 285-nm-wide trough with perfectly aligned cylindrical domains. The mild variation in the trough width along its length is accommodated by the polymer allowing perfectly aligned, defect-free cylindrical domains. This sample prepared by spin-coating the 1.55% polymer at 5 krpm is annealed at 408 K for 10 h.

the average trough width is 290.5 nm; hence, there are 10 PEP domains in the channel, but when the trough width near spot B increases to 313.8 nm, a dislocation is created and the number of PEP domains increases to 11. Between spot B and spot C, the trough width stays within the range for 11 domains; however, at spot C, when the width (271 nm) again becomes smaller than this range, another dislocation is created and the number of domains returns to 10. The plot in Figure 8a enables one to predict the behavior of confined cylindrical domains even when there are significant variations in the trough width.

Larger variations in the trough width can create interesting defect structures, particularly for narrower channels. The trough shown in Figure 10 has a periodic variation in its width; as a result, the number of PEP domains varies periodically from 7 (A) to 8 (B) with wider regions between these areas. The result of this variation is the periodic formation of a similar dislocation structure, emphasized by dashed circles in Figure 10. While careful preparation of the lithographically prepared gratings is vital to create defect-free polymer structures, such topographic imperfections can also be utilized to intentionally generate tailored defects at desired locations or to form periodic arrays of defects.

The average thickness of the polymer brush layer is 25.6 nm. Using this thickness and the equilibrium cylinder spacing of 26.6 nm, the ideal trough width for a given number of PEP domains can be calculated; the dashed lines in Figure 8a represent these equilibrium trough widths. The dashed lines are approximately centered

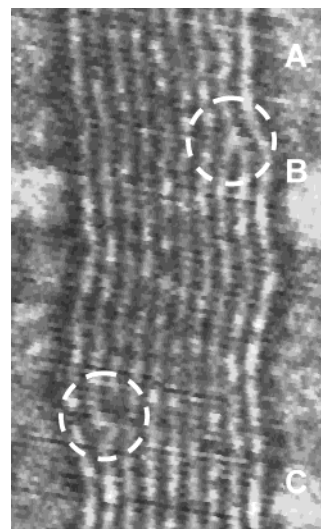


**Figure 9.** Thin film sample prepared by spin-coating the 1.55% polymer solution at 5 krpm on a 95-nm-deep grating and then annealing at 403 K for 30 h. The change in the number of PEP domains and the creation of defects due to variations in the trough width along its length is observed in this tapping mode phase AFM image. Ten dark domains are present near spot A (trough is 290.5-nm-wide). The number of dark domains increases to 11 near spot B (313.8 nm) while creating a dislocation. Near spot C (271 nm), the number of domains returns to 10 by creating another dislocation. Defects are highlighted in the dashed circles.

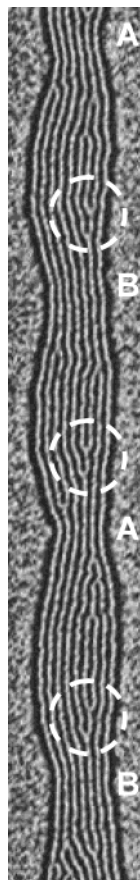


**Figure 10.** Significant variations in the trough width can create interesting defect structures as shown in this tapping mode phase AFM image. The number of PEP domains varies periodically from 7 (A) to 8 (B) as a result of periodic variations in the trough width. Similar defect structures, shown by dashed circles, are created.

within the accessible width ranges for each integer value of PEP domains. Maximal expansion and compression of the polymer are both approximately 10%, suggesting that steric repulsion within the polymer is energetically comparable with the entropic cost of extending the polymer strands. The system accommodates variations in the trough width by changing the cylinder size, matrix size, and brush layer thickness to varying degrees. Because PEP is softer than PS, we suspect that the PEP matrix is more pliable and accepts a larger part of the compliance responsibility; further studies are underway to ascertain the relative responses of each of the polymer components within confinement. Any change in the spacing beyond the maximum limits leads the system to attain a lower energy state by increasing or decreasing the number of polymer domains across the trough. In comparison to the spherical domain system studied by Cheng et al.,<sup>3</sup> the cylindrical domains studied here are more willing to stretch or compress in response to variations in the confining barriers. This is presumably due to the higher energetic cost of defect creation in cylindrical diblock films.

The alignment of cylinders is not limited to linear geometries. While straight domains have potential electronic and sensor applications, the available functions of templates with arbitrary morphology are far wider. Figure 11 depicts the ends of two neighboring channels. Rather than having angular corners, the trough termini are characteristically rounded. Impressively, the polymer cylinders follow the curved interface with minimal in-

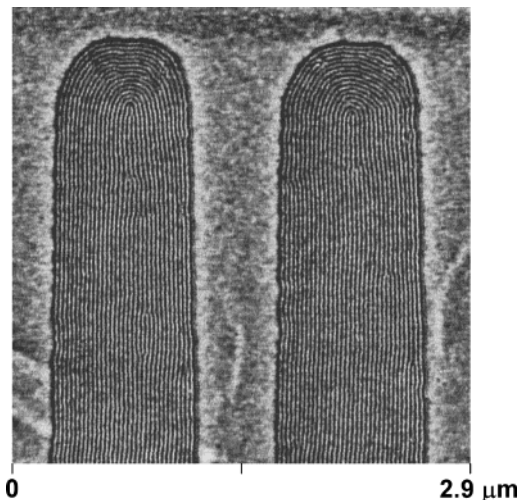
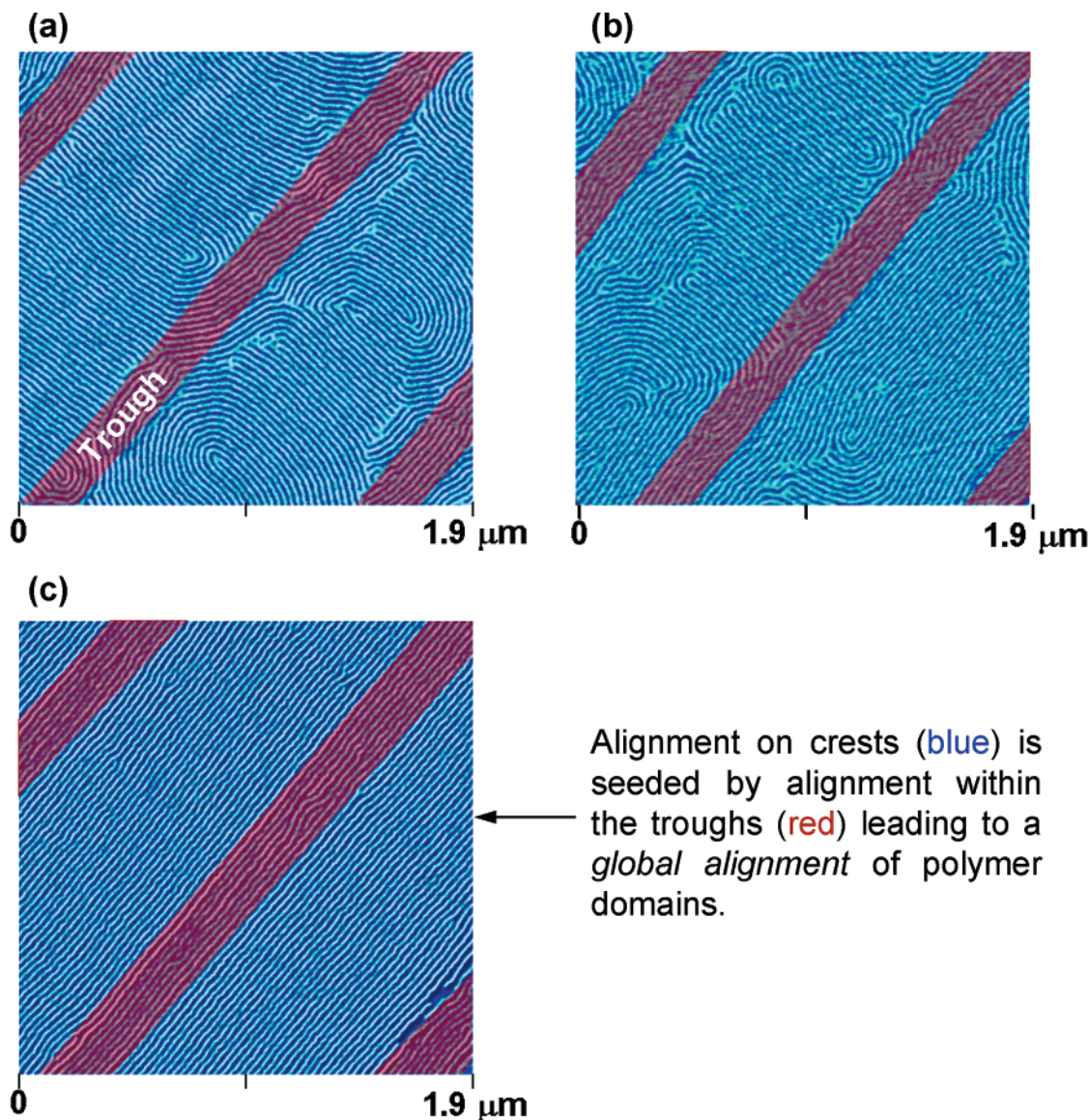


**Figure 11.** Thin film sample prepared by spin-coating the 1.55% polymer solution at 5 krpm on a 95-nm-deep grating and then annealing at 403 K for 30 h. Tapping mode phase AFM image,  $2.9 \mu\text{m} \times 2.9 \mu\text{m}$ , showing the aligned cylinders following the curvature of the trough ends. These troughs are 900-nm-wide, and the radius of curvature of the trough ends is 460 nm.

roduction of defects. The radius of curvature for these boundaries is 460 nm, or roughly 20 times the polymer domain spacing. Similar results have been observed for a variety of radii of curvature, and further studies are underway to ascertain the behavior of such films in more complex geometries.

**Alignment Beyond Confined Volumes.** When a grating is coated with a film thicker than the channel depth, several noteworthy phenomena are observed. Under certain conditions, crests can be prepared with a  $3L/2$ -thick film. During initial annealing of this sample at 408 K, the polymer flows from the crests into the troughs. This flow aligns the cylinders across the crests as shown in Figure 12a. Previously, perpendicular alignment of cylinders has been observed on small  $3L/2$ -thick islands on the crests,<sup>10</sup> but in this experiment, the cylinders are aligned across the long, continuous strips of  $3L/2$ -thick film present on the crests. The height difference from  $3L/2$ -thick (35 nm) film on the crests to the troughs is 3–4 nm, so the troughs are overfilled with the polymer and have an  $11L/2$ -thick (126 nm) film. At this stage of annealing, the cylinders in the troughs are largely aligned parallel to the grating lines. The top layer of cylinders in these channels is above the confined volume of the troughs, but the underlying cylinders extend the alignment to the cylinders in the highest layer.

Alignment of cylinders parallel to the grating lines in the channels can also induce parallel alignment of cylinders on the crests.<sup>13</sup> Figure 12b shows an image of a different spot on the same sample when annealed at 408 K for 6 h more. Now, the parallel alignment of the cylinders has nucleated at several locations on the crests. Further annealing of this sample (403 K for 20 h) leads to merging of these smaller aligned regions resulting in perfect parallel alignment of the cylinders on the crests (Figure 12c). This process demonstrates that the alignment of underlying cylinders in the troughs can not only induce alignment of cylinders above the confined channel volume, but it can also induce the lateral alignment of cylinders beyond the volumes of the troughs. This technique potentially can be extended to cause alignment of nanoscale polymer domains *across a complete surface*.



Alignment on crests (blue) is seeded by alignment within the troughs (red) leading to a *global alignment* of polymer domains.

**Figure 12.** Demonstration of the ability of alignment within the channels to induce global alignment across the entire surface. Sequential tapping mode phase AFM images of a thin film sample prepared by spin-coating the 1.55% polymer solution at 3.5 krpm on a 95-nm-deep grating and annealing at 408 K for (a) 6 h ( $2 \mu\text{m} \times 2 \mu\text{m}$ ) and (b) 12 h ( $1.9 \mu\text{m} \times 1.9 \mu\text{m}$ ) and then at (c) 403 K for 20 h ( $2.15 \mu\text{m} \times 2.15 \mu\text{m}$ ). The troughs have an  $11L/2$ -thick film whereas crests have a  $3L/2$ -thick film. The corrugation from the crests to the troughs is 3–4 nm.

### Conclusion

In this paper, we report a new methodology for aligning nanoscale cylindrical diblock copolymer domains over macroscopic length scales. This approach merges top-down and bottom-up methods to achieve long-range order while maintaining the advantages of self-organization. Alignment is initiated by a preferential wetting layer of PS on the vertical sidewalls of the lithographic channels and is extended throughout, and even beyond, the confined volume via coarsening of these edge-aligned domains. Higher coverage of polymer can also induce alignment of cylinders on the crests, thereby enabling alignment across an entire interface. Cylinders guided to align in this manner exhibit significant compliance that allows them to accommodate lithographic imperfections without introducing structural defects. Ramifications of this work extend to hybrid hard/soft condensed matter systems for

applications in electronics, catalysis, optics, tribology, and sensor technology.

**Acknowledgment.** We gratefully acknowledge Thomas Witten and Vladimir Belyi for useful discussions and Luping Yu, Dong-Chan Lee, and Qin Zheng for their preparation and characterization of the source polymer. This work was primarily supported by the University of Chicago-Argonne National Laboratory Consortium for Nanoscience Research. Work at Argonne was supported by the U.S. Department of Energy, Basic Energy Sciences-Materials Sciences, under Contract No. W-31-109-ENG-38. Support is also acknowledged from the NSF-Materials Research Science and Engineering Center at The University of Chicago, NSF-DMR-0213745. Further support for instrumentation development is acknowledged from the Air Force Office of Scientific Research.